BNL-90851-2009-CP

Simulation of Electric Field in Semi Insulating Au/CdTe/Au Detector Under Flux

J. Franc, R. Grill, R. James, J. Kubat, E. Belas, P. Hoschl, P. Moravec, and P. Praus

Presented at the SPIE Optics and Photonics
San Diego, CA
August 2-6, 2009

December 2009

Nonproliferation and National Security Department
Detector Development and Testing Division

Brookhaven National Laboratory
P.O. Box 5000
Upton, NY 11973-5000
www.bnl.gov

Notice: This manuscript has been authored by employees of Brookhaven Science Associates, LLC under Contract No. DE-AC02-98CH10886 with the U.S. Department of Energy. The publisher by accepting the manuscript for publication acknowledges that the United States Government retains a non-exclusive, paid-up, irrevocable, world-wide license to publish or reproduce the published form of this manuscript, or allow others to do so, for United States Government purposes.

This preprint is intended for publication in a journal or proceedings. Since changes may be made before publication, it may not be cited or reproduced without the author's permission.

DISCLAIMER

This report was prepared as an account of work sponsored by an agency of the United States Government. Neither the United States Government nor any agency thereof, nor any of their employees, nor any of their contractors, subcontractors, or their employees, makes any warranty, express or implied, or assumes any legal liability or responsibility for the accuracy, completeness, or any third party's use or the results of such use of any information, apparatus, product, or process disclosed, or represents that its use would not infringe privately owned rights. Reference herein to any specific commercial product, process, or service by trade name, trademark, manufacturer, or otherwise, does not necessarily constitute or imply its endorsement, recommendation, or favoring by the United States Government or any agency thereof or its contractors or subcontractors. The views and opinions of authors expressed herein do not necessarily state or reflect those of the United States Government or any agency thereof.

Printed on recycled paper

Simulation of electric field in semi insulating Au/CdTe/Au detector under flux

J. Franc*, R. Grill, R. James[&], J. Kubát, E. Belas, P. Hoschl, P. Moravec, P. Praus
*Institute of Physics, Charles University, Prague CZ 121 16, Czech Republic
[&]Brookhaven National Laboratory, Upton, New York 11973, USA

ABSTRACT

We report our simulations on the profile of the electric field in semi insulating CdTe and CdZnTe with Au contacts under radiation flux. The type of the space charge and electric field distribution in the Au/CdTe/Au structure is at high fluxes result of a combined influence of charge formed due to band bending at the electrodes and from photo generated carriers, which are trapped at deep levels. Simultaneous solution of drift-diffusion and Poisson equations is used for the calculation. We show, that he space charge originating from trapped photo-carriers starts to dominate at fluxes 10^{15}-10^{16}cm^{-2}s^{-1}, when the influence of contacts starts to be negligible.

Keywords: CdTe, detectors, recombination

1. INTRODUCTION

Charge collection efficiency in CdTe and CdZnTe X-ray and gamma ray detectors is influenced by a profile of the electric field in the detector and its time evolution. The Pockels electro-optic effect is frequently used to study the electric field distribution in the volume of the devices [1-3]. The profile of the electric field is governed by the space charge accumulated at deep levels. Accumulation of positive space charge resulting in an increased electric field near the cathode was observed in CdZnTe [1-3]. In Ref.3 also lateral distortion of the field was investigated. On the contrary, CdTe has a tendency to accumulate negative space charge (electric field is decreased near the cathode) [4]. A review of defects in wide band gap II-VI materials was presented in [5] [6] and the state-of-the-art of crystal growth and device fabrication technology was presented in [7-12].

The type of the space charge and electric field distribution in the Metal/CdTe/Metal structure is at low fluxes mostly influenced by the charge present due to the band bending near the electrodes the electrodes. The distribution of charge depends on the band bending at the metal/semiconductor interface, on the concentration of deep levels and on the applied voltage. Additional space charge originating from trapped photo carriers is accumulated with an increasing photon flux at deep levels further modifying the profile of the electric field. The nature of polarization due to space charge built-in the X-ray detectors operating at high fluxes was recently described in Ref. [13]. Here, however, the space charge formed below the electrodes due to the band bending was not included in the calculation.

The purpose of the present paper is to simulate distribution of the electric field in the metal/CdTe/metal structure in dependence of the flux of incoming radiation in order to estimate the potential influence of contacts on operation of CdTe and CZT detectors under high fluxes of X-ray photons. Gold was chosen for this simulation, nevertheless the same approach can be applied to other types of contact metals as well.

Gold represents one of the most optimal materials for formation of non injecting and non blocking contacts on semi insulating CdTe and CZT. The work function of Au Φ_{Au} is ~5.4eV [14], while the work function in semi insulating CdTe is in the range of 5.2-5.4eV depending on the position of the Fermi level in the near midgap region. The diagram showing the separated band scheme of Au and semi insulating CdTe is presented in Fig.1. The energy range of Fermi level position is depicted as dashed belt. In the case, that the CdTe is slightly n-type, the bends at the interface are bended upwards and positive space charge is present in the volume of CdTe. The opposite case occurs for slightly p-type

semi insulating CdTe. The average band bending characterizing also the case of semi-insulating CZT (10% of Zn, energy gap at room temperature ~1.58eV) can be estimated to 150-200meV. Band bending of 150meV was chosen for the simulation set presented in this paper.

A simple model consisting with one deep levels, which is characterized by ionization energy and electron and hole capture cross-sections, simulates the photoconductivity. A standard Shockley-Read model describes the recombination through the levels. The approach used here is an extension of the model in Ref. [15] in which only single principal deep level was taken into account.

The photoconductivity is simulated in a homogeneous planar sample with thickness L biased by a voltage U and characterized by Fermi energy E_F, which yields equilibrium electron and hole density before illumination n_0 and p_0, respectively. The considered deep levels with densities Ni, i is the level's index (i=1,2,...), are described by ionization energies E_i and electron and hole capture cross-sections $\sigma_{i,n}$ and $\sigma_{i,p}$.. Note that the character of the deep level (charge, donor or acceptor) does not stand directly in the theoretical forms.

The calculation is based on the self-consistent steady state solution of electron and hole drift-diffusion equations using an iterative method. The effect of space charge on the electric field distribution and carrier transport through the sample is evaluated by solving the Poisson equation. The electron and hole equilibrium in the steady photo excited system is described by equations

$$0 = \Phi \alpha e^{-\alpha x} + \mu_n \left[\frac{k_b T}{e} \frac{\partial^2 n}{\partial x^2} + \frac{\partial}{\partial x}(Fn) \right] - R \tag{1}$$

$$0 = \Phi \alpha e^{-\alpha x} + \mu_p \left[\frac{k_b T}{e} \frac{\partial^2 p}{\partial x^2} - \frac{\partial}{\partial x}(Fp) \right] - R \tag{2}$$

where Φ is photon flux, α is absorption coefficient, and μn(p) is the electron (hole) drift mobility. Einstein relation eD=kbTμ is used to express the diffusion term with mobility μ. Carrier recombination R is described within the Hall-Shockley-Read model.

$$R = (np - n_0 p_0) \sum_i \frac{c_n^{(i)} c_p^{(i)} N_i}{c_n^{(i)}(n + n_1^{(i)}) + c_p^{(i)}(p + p_1^{(i)})} \tag{3}$$

The capture coefficients are defined by with electron (hole) thermal velocity v_n (v_p) and $n_1^{(i)}$, $p_1^{(i)}$ are electron and hole densities when the Fermi level $c_{n(p)}^{(i)} = \sigma_{i,n(p)} v_{n(p)}$ is set to E_i.

Electric field

$$F = -\frac{\partial \varphi}{\partial x} \tag{4}$$

and electrochemical potential φ are obtained by solving Poisson equation

$$\frac{\partial^2 \varphi}{\partial x^2} = -\frac{\rho}{\varepsilon} \tag{5}$$

with boundary conditions φ(0)=0 and φ(L)=U. The charge density ρ is given by the change of the band and level occupation

$$\rho = e\left(p - p_0 - n + n_0 - \sum_i (n_t^{(i)} - n_{t0}^{(i)}) \right) \tag{6}$$

where $n_t^{(i)}$ and $n_{t0}^{(i)}$ define deep level occupation,

$$n_t^{(i)} = \frac{N_i \left(c_n^{(i)} n + c_p^{(i)} p_1^{(i)} \right)}{c_n^{(i)} \left(n + n_1^{(i)} \right) + c_p^{(i)} \left(p + p_1^{(i)} \right)} \tag{7}$$

$$n_{t0}^{(i)} = \frac{N_i}{1 + e^{\left(E_i - E_F \right) / k_b T}} \tag{8}$$

The variation in the occupation of shallow levels is neglected. Boundary conditions are set by Fermi energy pinned to EF in metal, which yields the band bending at the surface $E_{cs}(E_{vs})- E_c(E_v)=-\Phi_{CdTe}+\Phi_{Au}$. The surface carrier density is than fixed as

$n(0)=n(L)=n_0 \exp (\Phi_{CdTe}-\Phi_{Au})k_bT$

and

$p(0)=p(L)=p_0 \exp- (\Phi_{CdTe}-\Phi_{Au})k_bT$.

Eqs. (1), (2) are solved numerically by an iterative method. Both dark current J0 and photocurrent Jph are constant through the sample and the photocurrent is expressed by

$$Jph=e[\mu_n n(x)+\mu_p p(x)]F(x)- e[\mu_n n'(x)+\mu_p p'(x)]F'(x), \tag{9}$$

where quantities at dark are prime labeled.

While the presented set of equations is valid for an arbitrary number of levels, one deep level was used to simulate the results presented in this paper. Typically, the complicated nonlinear character of solved equations (1), (2), and (5) results in a slow convergence of the iterative method with strong tendency to oscillate. As it is usual in such situations, the oscillations are effectively damped by averaging successive iterations, when the new iteration is involved only with a weight of several percent.

3. SIMULATION PARAMETERS

Due to the fact, that simulation results in principle depend on parameters of deep levels, it is important to work with parameters representing conditions present in state of the art detectors.

The observed concentrations of deep levels in semi-insulated CdTe and (CdZn)Te are low. In Ref. [16] 0.6-0.7eV levels with $N\sim10^{11}$-$10^{13}cm^{-3}$ were deduced from the time dependence of discharge current after an X-ray pulse. Concentrations of levels between 10^{11}-$10^{12}cm^{-3}$ were used in Ref.[13] to explain charge buildup in CdZnTe detectors under high fluxes of photons. Also Cola et al. [17] evaluated concentrations of space charge between 10^{11}-$7x10^{11}cm^{-3}$ from the slope of electric field profile. Therefore, we use the parameters of midgap level from Ref. [13], which is consistent with experimentally observed charged transport properties of fully compensated semi-insulating CZT. The parameters are shown in Table 1 for the whole set of simulations presented in the paper. The calculations were done for two values of absorption coefficient α=40000 and α=50. The first value represents high absorption, which takes place at illumination with light of above-band gap energy. The second value characterizes illumination with medium-energy X-rays or with an infrared laser.

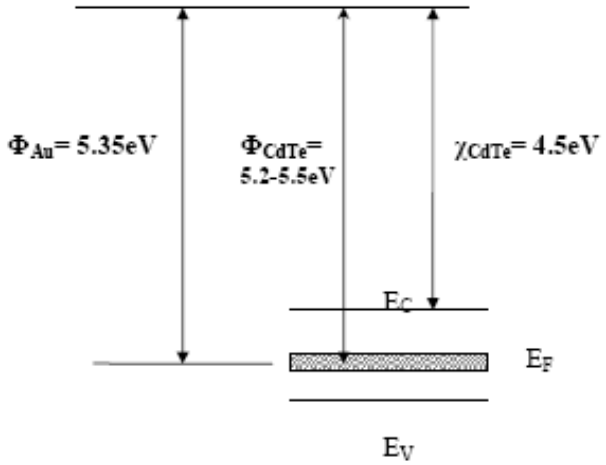

Fig. 1. Band scheme of the Au/CdTe system.

4. RESULTS

4.1. $\Phi_{CdTe} < \Phi_{Au}$

Results of simulations, which include one midgap energy level will be presented. Fig.2a shows the profile of space charge of the Au/CdTe/Au structure without illumination for the slightly p-type CdTe, when the work function of CdTe Φ_{CdTe}=5.2eV< Φ_{Au}=5.35eV (simulation no.1). Positive space charge due to the band bending extends to approx. 100μm. When 10V are applied on the structure (positive voltage on the anode), the space charge in the volume increases and its profile is asymmetrical due to increased band bending. At the standard operating voltage of detectors (100V applied on 1mm thick sample) almost the whole volume of detector is influenced by positive charge. Corresponding profiles of electric field are presented on Fig.2b. Gradual increase of the field near the cathode with increasing applied voltage is apparent.

Fig.3a shows results of dependence of profile of electric field (applied voltage 100V, absorption coefficient α=40000) on the radiation flux illuminating the cathode (simulation No.2). The profile is gradually changing with an increasing flux. Electron-hole pairs are created just below the cathode. While electrons drift in the field to the anode and are trapped at the deep level, holes recombine immediately at the cathode. Negative space charge formed due to electron trapping neutralizes the positive space charge injected from contacts at a flux 10^{12}-10^{13}cm^{-2}s^{-1}, when constant electric field is achieved throughout the sample. Further increase of the flux results in a decreased electric field near the cathode.

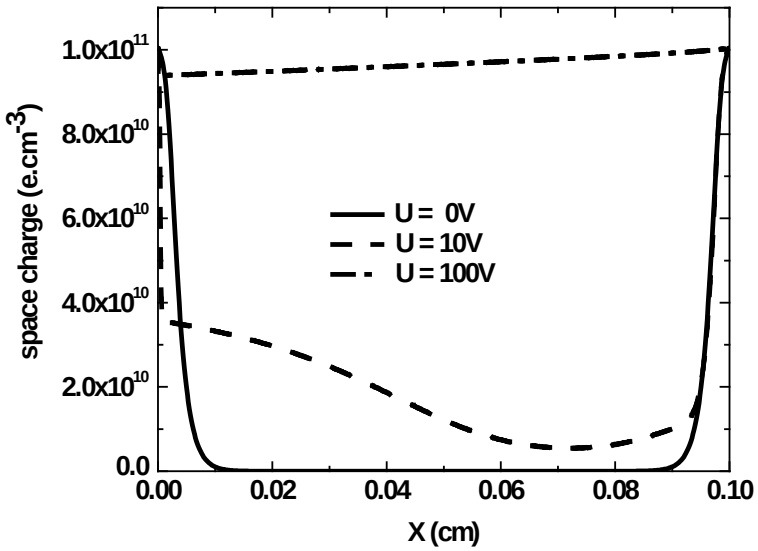

Fig.2a Profile of space charge density in units of elementary charge for the situation when positive space charge is formed due to band bending at the electrodes -simulation No.1).

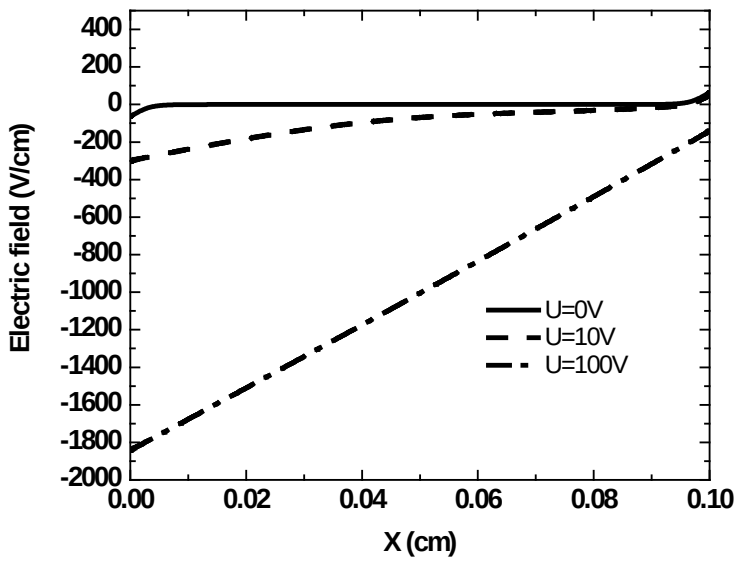

Fig.2b Profile of electric field for the situation when positive space charge is formed due to band bending at the electrodes -simulation No.1).

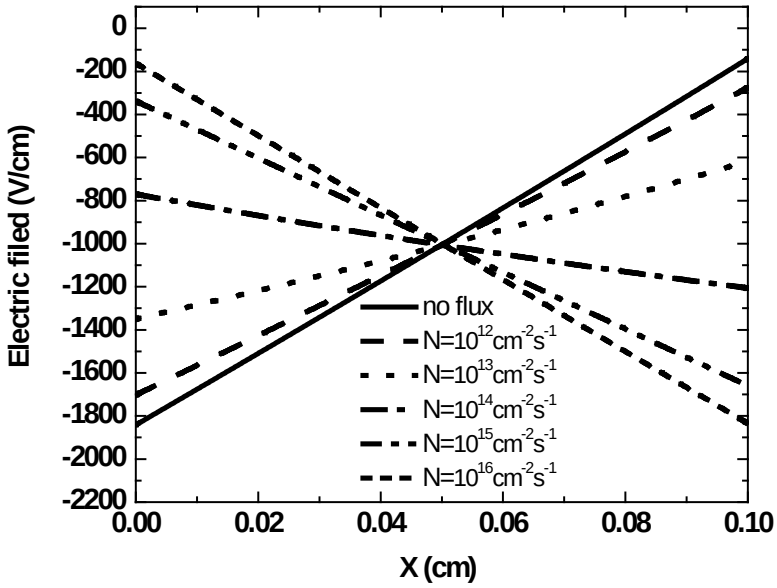

Fig.3a - dependence of profile of electric field (applied voltage 100V, absorption coefficient α=40000) on the radiation flux illuminating the cathode (simulation No.2).

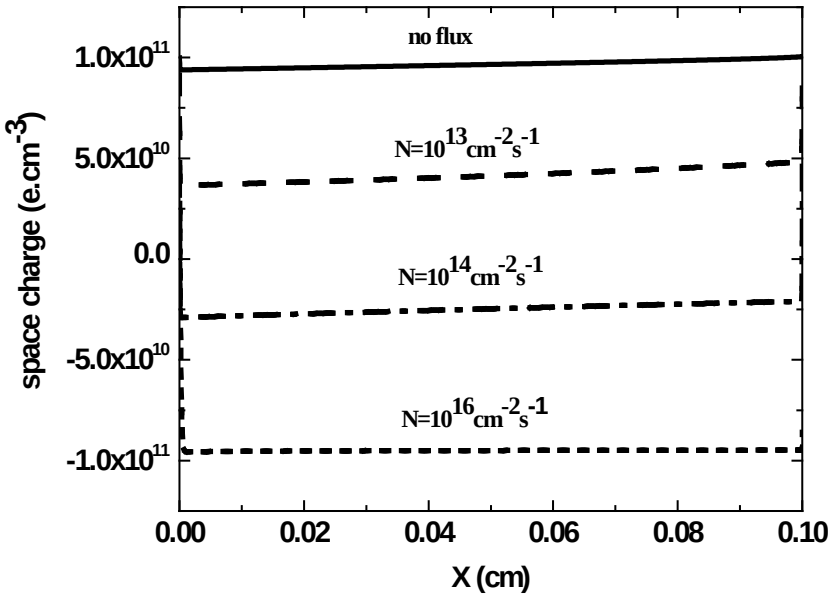

Fig.3b Corresponding profiles of space charge in units of elementary charge in dependence of the flux.

The corresponding profiles of space charge in units of elementary charge in dependence of the flux are shown in Fig.3b. Fig.4 then depicts profile of electric field for flatband conditions at both metal/semiconductor interfaces (simulation no.3). In this case no space charge is formed due to band bending at the contacts and the distortion of electric field is completely caused by the trapped charge originating from radiation induced photo carriers. The profile of the field with the discussed band bending is approached at flux $10^{15}cm^{-2}s^{-1}$. These results are important for the study of photoconductivity with light with energy higher than the bandgap. Small band bending (injection of positive space charge from contacts) does not influence the photoconductivity signal at high photon fluxes.

Let us now discuss the case interesting for X-ray radiation detectors at high fluxes. This situation is in the current simulation represented by a small absorption coefficient α. The distribution of electric field for the same case as discussed above (small band bending downwards-injection of positive space charge from both contacts), but with α=50 is presented in Fig.5a (Simulation no.4). The same evolution of the slope as in Fig. 3a can be seen up to the flux $\sim 10^{14}cm^{-2}s^{-1}$. Then a minimum in the field distribution starts to develop. This effect was in detail described in Ref.[5], where this extreme was named the "pinch point". Holes traveling from the generation point to the cathode are trapped left to the pinch point, while electrons are trapped in the region between the pinch point and the anode. The sample is then divided into two oppositely charged parts. The distribution of space charge in the sample in dependence of the radiation flux is presented on Fig.5b. Fig.6 shows comparison of electric field profiles for the small band bending and for flatband conditions at both contact interfaces. It is apparent, that even a small band bending influences the formation of pinch point and its position within the detector.

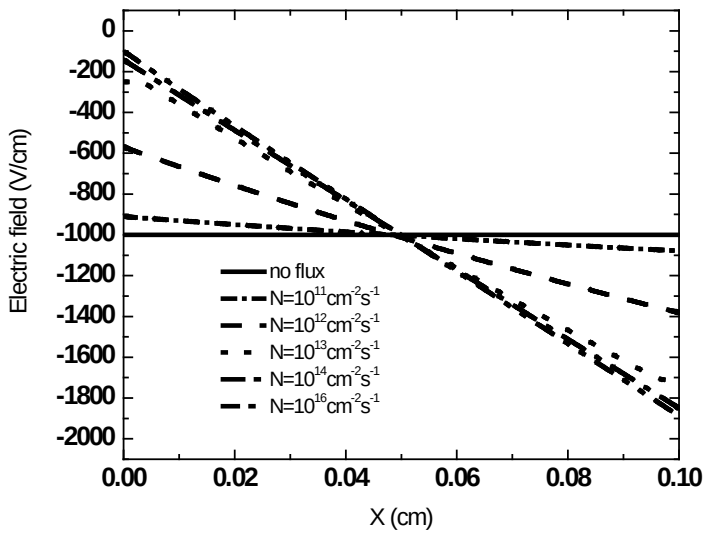

Fig.4 Profile of electric field for flatband conditions at both metal/semiconductor interfaces (simulation no.3).

4.2. $\Phi_{CdTe} > \Phi_{Au}$

In the next section we will discuss the case of slightly p-type semi insulated CdTe (Φ_{CdTe}=5.5eV> Φ_{Au}= 5.35eV. The bands at both interfaces are bended downwards; negative space charge is formed at the electrodes. Fig.7a shows the profile of space charge of the Au/CdTe/Au (simulation no.5). In Fig.7b corresponding profiles of electric field can be seen. Inverse situation to that described in Figs 2a,b takes place. The negative space charge in the volume increases with the increase of applied voltage. Its profile is asymmetrical due to increased injection of electrons from the cathode and at 100V almost the whole volume of detector is influenced by negative space charge.

Fig.8 shows the electric field profile in dependence of the radiation flux falling at the cathode for the case of the high absorption coefficient (simulation no.6). The sample is flooded by negative space charge without irradiation. This

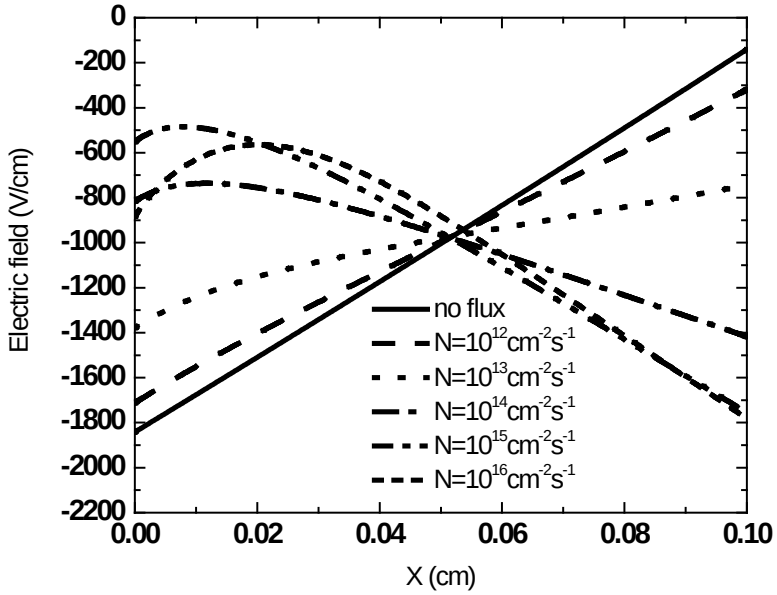

Fig.5a The distribution of electric field (positive space charge present due to bend bending at both contacts), for α=50 in dependence of the radiation flux (Simulation no.4).

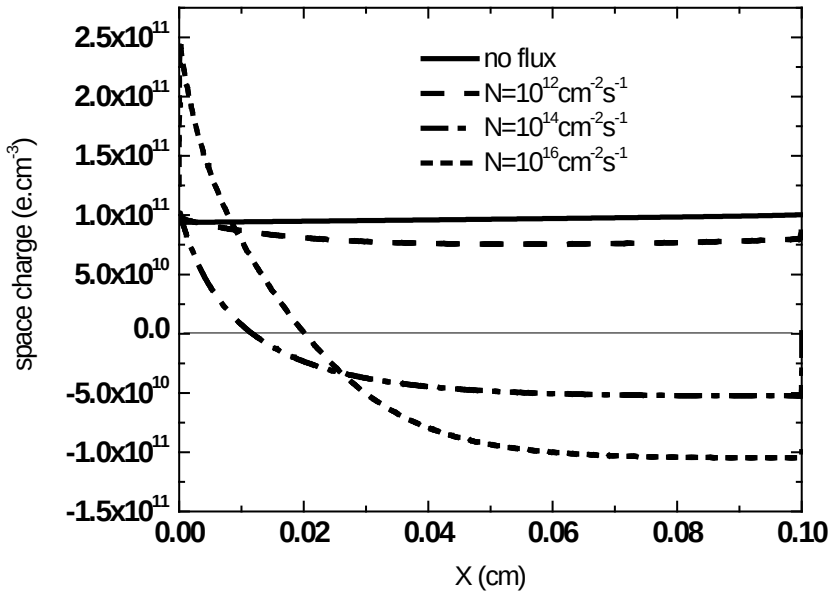

Fig.5b The distribution of space charge for α=50 in dependence of the radiation flux (Simulation no.4).

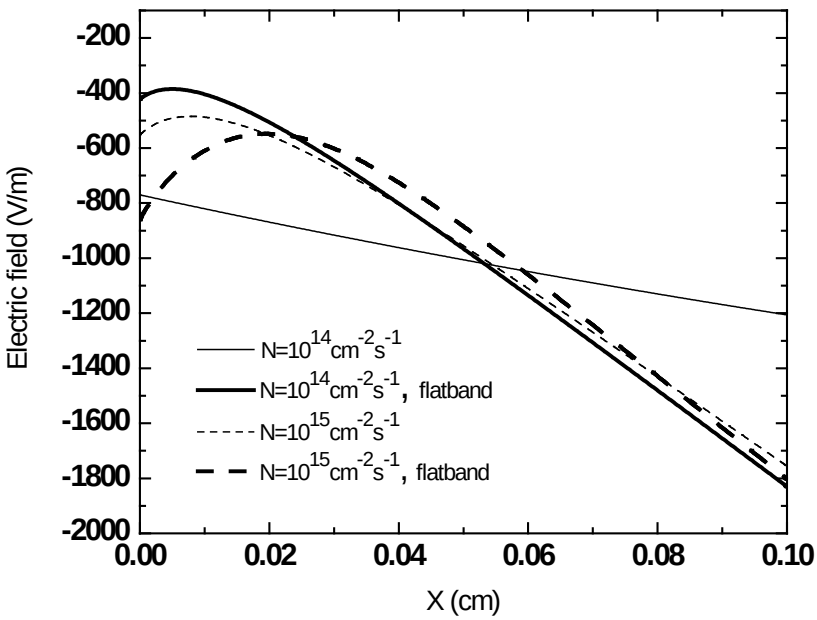

Fig.6 Comparison of electric field profiles for the small band bending and for flatband conditions at both contact interfaces

space charge dominates up to a very high flux of incident radiation -10^{15}-10^{16}cm^{-2}s^{-1}, when the additional negative space charge from trapped electrons at the deep level starts to be comparable with the charge due to band bending. The electric field strength below the cathode then continues to decrease. Fig.9a represents the same case of bend bending with the low absorption coefficient α=50cm^{-1} (simulation no.7). The evolution of the pinch point similar to Fig.5a can be seen. The profiles of the field at fluxes 10^{14} and 10^{15} cm^{-2}s^{-1} are compared to the ideal situation of flatband conditions at both interfaces in Fig.9b. A significant difference in the position and electric field of the pinch point minimum at flux 10^{15}cm^{-2}s^{-1} is apparent. While under flatband conditions the pinch point is clearly seen and is located deep in the sample, band bending effectively stops its formation. The negative space charge formed at the electrodes prevails over the positive charge from trapped photo holes at this flux.

5. CONCLUSIONS

Profiles of electric field in detector-grade semiinsulating Au/CdTe/Au (Au/CdZnTe/Au) with a low concentration of midgap level (~10^{11}cm^{-3}) were simulated. The electric field in a non-irradiated sample is strongly distorted by space charge even at very small bend bending at the interfaces (<150meV). The space charge originating from trapped photo-carriers starts to dominate at fluxes 10^{15}-10^{16}cm^{-2}s^{-1}, when the influence of contacts starts to be negligible. Formation and position of electric field minimum (pinch point) is also influenced by contacts. The minimum can completely disappear with an increasing band bending.

5. ACKNOWLEDGEMENT

This paper is a part of the research plan MSM 0021620834 that is financed by the Ministry of Education of the Czech Republic. It was also financially supported by the Grant Agency of Charles University (No. 7692/2007) and Alexander von Humboldt foundation. One author (R.B. James) wishes to gratefully acknowledge support from the U.S. Department of Energy, Office of Nonproliferation Research and Engineering, NA-22.

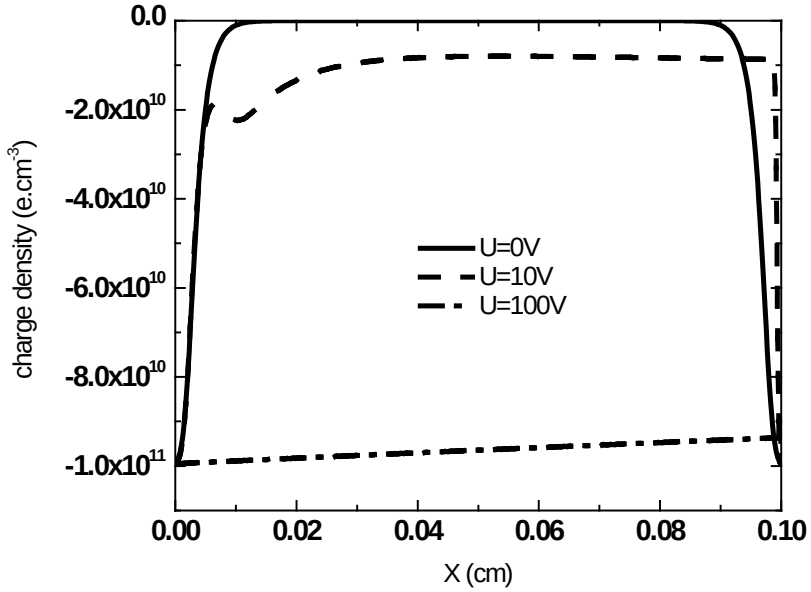

Fig.7a Profile of space charge density in units of elementary charge for the situation when negative space charge is formed due to band bending at the electrodes -simulation No.5).

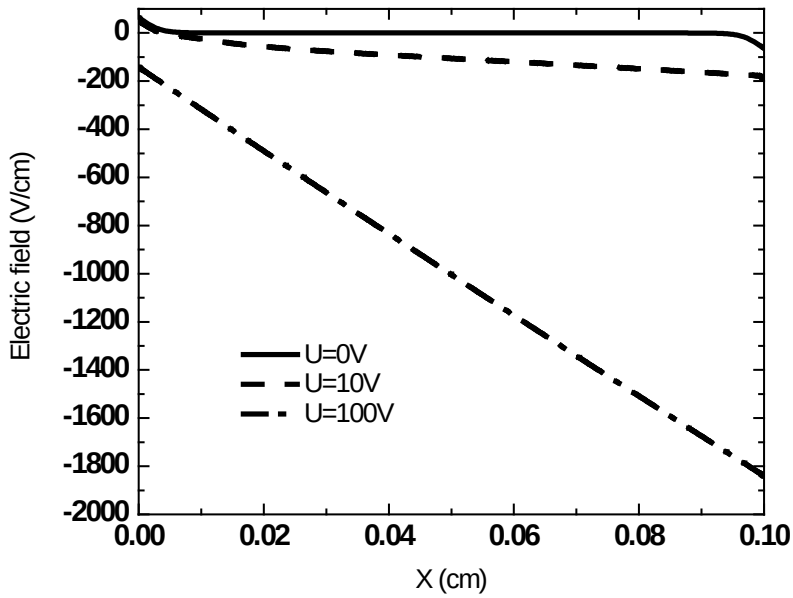

Fig.7b Profile of electric field for the situation when negative space charge is formed due to band bending at the electrodes -simulation No.5).

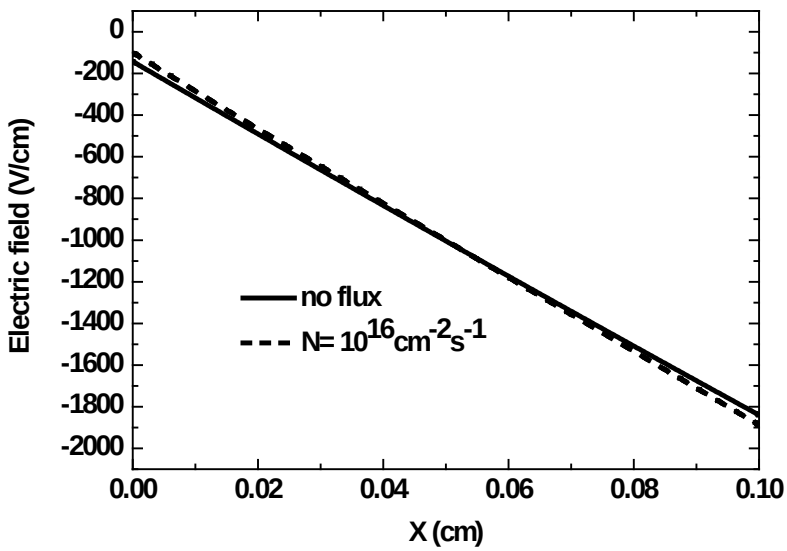

Fig.8 Electric field profile in dependence of the radiation flux falling at the cathode for the case of the high absorption coefficient (simulation No.6).

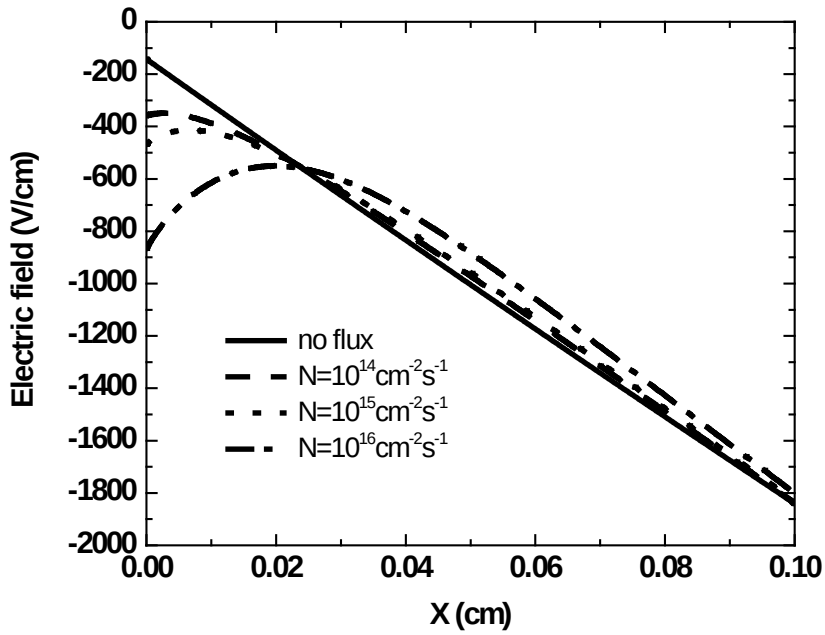

Fig.9a Profiles of the electric field for the case of injection of negative charge from electrodes (low absorption coefficient α=50cm^{-1} - simulation No.7).

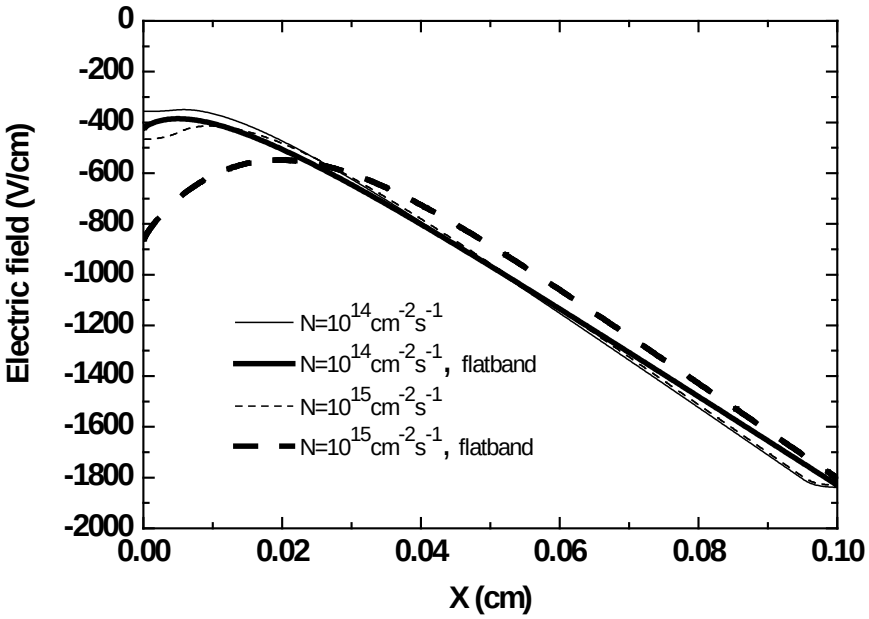

Fig.9b The profiles of the field at fluxes 1014 and 1015 cm-2s-1 compared with the ideal situation of flatband conditions at both interfaces.

Table 1List of parameters used in the simulations

No.	Φ_{Au}(eV)	Φ_{CdTe}(eV)	α(cm^{-1})	E_1	$\sigma_{1,e}$(cm^2)	$\sigma_{1,h}$(cm^2)	N_1(cm^{-3})	N_{fot}(cm^{-2}s^{-1})
1	5.35	5.20	-	$0.4E_g$	5×10^{-13}	3×10^{-14}	2×10^{11}	0
2	5.35	5.20	$4x10^4$	$0.4E_g$	5×10^{-13}	3×10^{-14}	2×10^{11}	0 -10^{16}
3	5.35	5.20	$4x10^4$	$0.4E_g$	5×10^{-13}	3×10^{-14}	2×10^{11}	10^8-10^{16}
4	5.35	5.20	50	$0.4E_g$	5×10^{-13}	3×10^{-14}	2×10^{11}	0 -10^{16}
5	5.35	5.50	-	$0.6E_g$	5×10^{-13}	3×10^{-14}	2×10^{11}	0
6	5.35	5.50	$4x10^4$	$0.6E_g$	5×10^{-13}	3×10^{-14}	2×10^{11}	10^{16}
7	5.35	5.50	50	$0.6E_g$	5×10^{-13}	3×10^{-14}	2×10^{11}	

REFERENCES

[1] [1] Hossain, M., A., Morton, E.,J., and Öszan, M.,E., "Photoelectric Investigation of CdZnTe Spectral Detectors", IEEE Trans.Nucl.Sci 49(4), 1960-1964 (2002).

[2] [2] Yao, H.,W., James R.,B., and Erikson,E.,C., "Optical Engineering and Characterization of the Internal Electric Field Distribution of CdZnTe Detectors", Proc.SPIE 3115, 62-68 (1997).

[3] [3] Bolotnikov,A.,E., Camarda,G.,S., Cui,Y., Hossain,A., Yang,G., Yao, H.,W., and James, R.,B., "Internal electric field lines distribution in CdZnTe Detectors measured using X-ray mapping", IEEE Trans.Nucl.Sci. 56(3), 791-794 (2009).

[4] [4] Cola,A., Farella,I., Mancini A.,M., and Donati,A., "Electric Field Properties of CdTe Nuclear Detectors", IEEE Trans.Nucl.Sci.54, 868-872 (2007).

[5] [5] Castaldini, A., Cavallini, A., Fraboni, B., Fernandez, P., and Piqueras, J., „Deep Energy Levels in CdTe and CdZnTe", J.Appl.Phys.83(4), 2121-2126 (1998).

[6] [6] Neumark,G.,F., „Defects in Wide Band Gap II-VI crystals" Mater.Sci.Eng.R21, 1-46, (1997).

[7] [7] Szeles,C., „CdZnTe and CdTe Materials for X-ray and Gamma Ray Radiation Detector Applications", Phys. Stat. Sol.(c) 241(3), 783-790 (2004).

[8] [8] Chen,H., Awadalla,S., Mackenzie,J., Redden,R., Bindley,G., Bolotnikov,A.,E., Camarda,G.,S., Carini,G., "Characterization of Travelling Heater Method (THM) Grown Cd0.9Zn0.1Te crystals", IEEE Trans. on Nucl. Sci. 54(4), 811-816 (2007).

[9] [9] Carcelen,V., Viayan,N., Dieguez,E., Zapettini,A., Zha,M., Sylla,L., Fauler,A., Fiederle,M., "New Approaches to Enlarge the Grain Size of Bulk CdZnTe (CZT) crystals", J.Optoelectronics and Advances Materials 10(11), 3135-3140 (2008).

[10] [10] Saucedo,E., Rudolph,P., and Dieguez,E., "Modified Bridgman Growth of CdTe crystals", Journal of Crystal Growth 310(7-9), 2067-2071 (2008).

[11] [11] Chen,H., Awadalla,S., Harris,R., Lu,P.,H., Redden,R., Bindley, G., Copete,A., Hong,J., Gridlay,J., Amman,M., Lee,J.,S., Luke,P., Kuwetli,I., Budtz-Jorgensen,C., "Spectral Response of THM Grown CdZnTe crystals", IEEE Trans.Nucl.Sci. 55(3), 1567-1572 (2008).

[12] [12] Shiraki,S., Funaki,M., Ando,Y., Kominami,S., Amemiya,K., Ohno,R., 2007 IEEE Trans.Nucl.Sci. Conference Records, vols.1-11, pp.1783-1787, (2007).

[13] [13] Bale,D.,S., Szeles,Cs., "Nature of Polarization in Wide Band-Gap Semiconductor Detectors under High-Flux Irradiation: Application to Semi-Insulating CdTe", Phys.Rev.B 77, Art.No.035205 (2008).

[14] [14] CRC Handbook on Chemistry and Physics, CRC Press (New York,), David R.Lide, editor, 12-124 (1999)

[15] [15] Brinkman, A.,W., [Properties of Narrow Gap Cadmium based Compounds], EMIS Datareviews Series No.10, INSPEC, 575-576 (1994).

[16] [16] Jahnke,A., Matz,R., „Signal Formation and Decay in CdTe X-ray Detectors", Med. Physics 26, 38-48 (1999).

[17] [17] Cola,A., Farella,I., Mancini,A.,M., Donati,A., "Electric Field Properties of CdTe Nuclear Detectors", IEEE.Trans.Nucl.Sci. 54, 868-872 (2008).